Increased dust aerosols in the high troposphere over the Tibetan Plateau from 1990s to 2000s

Xingya Feng[1,2], Rui Mao[1,2,3*], Daoyi Gong[1,2,3], Chun Zhao[4], Chenglai Wu[5], Chuanfeng Zhao[6], Guangjian Wu[7], Zhaohui Lin[5], Xiaohong Liu[8], Kaicun Wang[6], Yijie Sun[1,2]

[1] Key Laboratory of Environmental Change and Natural Disaster, Ministry of Education, Beijing Normal University, Beijing 100875, China

[2] Academy of disaster Reduction and Emergency Management, Faculty of Geographical Science, Beijing Normal University, Beijing, China

[3] State Key Laboratory of Earth Surface Processes and Resource Ecology, Beijing Normal University, Beijing, China

[4]School of Earth and Space Science, University of Science and Technology of China, Hefei, China

[5]Institute of Atmospheric Physics, Chinese Academy of Sciences, Beijing, China

[6]College of Global Change and Earth System Science, Beijing Normal University, Beijing, China

[7]Institute of Tibetan Plateau Research, Chinese Academy of Sciences, Beijing, China

[8] Department of Atmospheric Science, University of Wyoming, Laramie, WY, USA

To be submitted to *Journal of Geophysical Research-Atmospheres*

March 2020

*Corresponding author: Rui Mao, mr@bnu.edu.cn

1

Key Points:

- The dust aerosols increased in the upper troposphere over the TP during 2000s compared to 1990s
- The increasing dust aerosols over the TP may be related to increasing dust emissions in the Middle East
- Enhanced zonal winds in the middle and high troposphere may transport more dust from the Middle East to the TP.

2

ABSTRACT

The dust aerosols are a major type of aerosol over the Tibetan Plateau (TP) and influence climate at local to regional scales through their effects on thermal radiation and snow-albedo feedback. Based on the Modern-Era Retrospective Analysis for Research and Applications, Version 2 (MERRA-2) aerosol dataset, we report an increase of 34% in the atmospheric dust in the high troposphere over the TP during the spring season in the 2000s in comparison to the 1990s. This result is supported by an increase of 157% (46%) in the dust deposition flux in the Mugagangqiong (Tanggula) ice cores and an increase of 69% in the Aerosol Index (AI) from Earth Probe (EP) Total Ozone Mapping Spectrometer (TOMS), as well as by increases of simulated dust aerosols over the TP derived from the Community Earth System Model (CESM) and models from the Coupled Model Intercomparison Project Phase 6 (CMIP6). The increased atmospheric dust over the TP is caused in two aspects: (1) there was a higher dust emission over the Middle East during the 2000s than during the 1990s, which is explained by less precipitation and 25.8% higher in cyclone frequency over the Middle East. The increased cyclones uplift more dust from the surface over the Middle East to the central Asia in the middle troposphere. (2) Enhanced mid-latitude zonal winds help transport more dust in the middle troposphere from the central Asia to the Northwest China and thereafter an increase in northerly winds over Northwest China propels dust southward to the TP.

Keywords: The Tibetan Plateau; Dust aerosols; Middle East; Ice core; CMIP 6

1. Introduction

As an important component of aerosols over the Tibetan Plateau (TP), dust aerosols play an important role in regional climate and environmental change (Chen et al., 2013; Huang et al., 2007; Liu et al., 2008; Mao et al., 2013; Zhao et al., 2020). Dust aerosols over the TP can affect climate by directly scattering solar radiation and absorbing longwave radiation from the surface and atmosphere. (Chen et al., 2013; Lau et al., 2006; Lau & Kim, 2018; Sun et al., 2017; Yang et al., 2018). For example, Chen et al. (2013) simulated a dust storm event that occurred during July 26-30, 2006, which originated from the Taklimakan Desert and transported dust to the north slope of the TP. The simulations showed that the event-averaged net radiative forcing modified the atmospheric heating profile over the TP with -3.97, 1.61, and -5.58 $W \cdot m^2$ at the top of the atmosphere, in the atmosphere, and at the surface, respectively. At a regional scale, the highly elevated surface air over the TP may act as an “elevated heat pump” through the absorption of solar radiation by dust coupled with black carbon emissions from industrial areas in north India. As a result, a tropospheric temperature anomaly may be induced in late spring and early summer over parts of north India and the TP, leading to an earlier onset and intensification of the Indian monsoon (Lau et al., 2006; Lau and Kim, 2018). Recently, Lau and Kim (2018) and Sun et al. (2017) verified the role of dust aerosols over the TP in influencing regional climate based on a dust-coupled global climate model. Sun et al. (2017) indicated that dust originating from the TP exerted a cooling effect in the mid-troposphere over the TP; thereafter an anticyclonic circulation anomaly centered over the TP region was simulated, which weakened the intensity of the East Asian summer monsoon through its northeasterly anomaly. Moreover, dust aerosols can influence cloud droplet concentration through acting as condensation nuclei in the cloud; therefore, the microphysical characteristics and life cycle of clouds can be changed, resulting in more complex and uncertain indirect effects (Forster et al., 2007; Han et al., 2009; Haywood et al., 2003; Huang et al., 2009, 2014). Thus, changes

in the amount of atmospheric dust over the TP are of great significance to evaluate the climate and human life on the TP (Lau et al., 2010; Qian et al., 2014; Sang et al., 2013).

Due to the scarcity of observations of atmospheric dust over the TP, changes in the dust during recent decades are unclear in the high troposphere over the TP. Dust aerosols over the TP originates from local and remote sources such as semiarid areas over the TP, the Taklimakan Desert, North Africa, the Middle East, Central Asia, and Southwest Asia (Huang et al., 2007; Jia et al., 2015; Liu et al., 2015; Mao et al., 2019). Based on the dust observations from surface meteorological stations, researchers have indicated that dust events over the TP have significantly decreased from 1960-2010 (Han et al., 2009; Kang et al., 2016). However, dust in the middle to high troposphere over the TP is mainly determined by remote sources rather than local sources (Mao et al., 2013; 2019). The contribution of local sources to the atmospheric dust over the TP decreases sharply with height, from 69% at the surface to 40% in the lower troposphere and 5% in the middle troposphere (Mao et al., 2013). Therefore, the changes in high-altitude dust over the Tibetan plateau may be different from those in the frequency of dust events at the surface. In contrast to dust event frequency, variations in the dust aerosols in the high troposphere over the TP can be elucidated by ice cores. The average annual deposition fluxes from Tanggula ice core and mugagangqiong ice core show an upward trend from 1990 to 2010 (Gong et al., 2012). This means that dust aerosols in the high troposphere over the TP may have increased during 2000s compared to 1990s.

In this study, we will examine the changes in the high tropospheric dust aerosols over the TP during past 20 years. In the meantime, possible mechanisms of the variations in the high tropospheric dust over the TP will be addressed. This paper is organized as follows. Section 2 provides a general description of the dataset and the method used in this study. In Section 3, we show increased dust aerosols in the troposphere over the TP during the 2000s compared with the 1990s. In Section 4, a significant contribution of remote dust sources to the increased dust aerosols over the TP during the 2000s is recognized. The causes of these increased dust aerosols over the

TP during the 2000s are clarified in Section 5. Discussion and conclusion are given in Section 6 and Section 7, respectively.

2. **Data and Method**

Two kinds of Reanalysis datasets were used in this study: the Modern-Era Retrospective Analysis for Research and Applications version 2 (MERRA-2) and the Japanese 55-year Reanalysis data set (JRA-55). The MERRA-2 is a dataset of earth observation system reanalysis for the satellite era using the Goddard Earth Observing System Model provided by NASA since 2014, and it has a relatively good temporal and spatial resolution that comprises a long-term record (Gelaro et al., 2017). Diop et al. (2018) used the MERRA-2 Reanalysis dataset to study seasonal distribution of dust dry deposition in West Africa particularly in Senegal. In this study, we used two MERRA-2 dust aerosol products: Aer-2D (monthly, dust optical thickness and dust emission) with a horizontal resolution 0.625°×0.5° and Aer-3D (3-hourly, dust mixing ratio) with a horizontal resolution of 0.625°×0.5°and 72 vertical levels. The JRA-55 dataset extends from 1958 to the present, with a horizontal resolution of 1.25°×1.25° and 37 vertical levels above the surface. The JRA-55 is based on a new data assimilation and prediction system that improves many deficiencies found in the first Japanese reanalysis (Kobayash et al., 2015). To explain dust transport from remote sources to the TP, we analyzed 6-hourly and monthly zonal wind, meridional wind, and vertical velocity from the JRA-55 dataset.

In order to verify the changes in the tropospheric dust over the TP, multiple data were employed in the analysis. (1) We used two ice core data from Mugagangqiong (MGGQ) (32.24°N, 87.48°E, drilled at 6085 m) and Tanggula (33.12°N, 92.08°E, drilled at 5743 m) in the central TP. These two ice core records provide dust deposition flux starting from 1850 to 2004 AD at Tanggula (Wu et al., 2013) and from 1950 to 2014 at MGGQ (Li et al., 2019). (2) A global dust simulation in 1979-2005 was run by the Community Earth System Model (CESM). The simulated monthly aerosol optical

depth at 550nm from dust was analyzed. The CESM is a flexible and extensible community tool that is employed to investigate a diverse set of earth system interactions across multiple time and space scales (Hurrell et al., 2013). The CESM incorporates many earth systems modeling capabilities, including the global dust cycle and the impact of dust on radiation, cloud, snow albedo, and biogeochemical cycles. The emission of dust particles into the atmosphere is calculated based on the scheme of the Dust Entrainment and Deposition Model (Zender et al., 2003). The CESM simulation was evaluated by simulating a typical severe dust storm in East Asia (including the TP) (Wu et al. 2016). (3) The monthly Aerosol Index (AI) from Earth Probe (EP) Total Ozone Mapping Spectrometer (TOMS) version 8 global data product was analyzed. The monthly AI data we used from August 1996 to March 2005 with a horizontal resolution 1.25°×1°. TOMS is most sensitive to aerosols in the middle and upper troposphere and in the stratosphere (Gao and Washington, 2010). Mao et al. (2013) used AI to reflect the change of dust aerosol in the upper troposphere over Tibetan Plateau. (4) Simulated dust concentration in the Atmospheric Model Intercomparison Project (AMIP) from the Coupled Model Intercomparison Project Phase 6 (CMIP6) was examined. Because the AMIP is constrained by realistic sea surface temperature and sea ice, the simulations focus on the influence of atmospheric circulation on dust aerosols without the added complexity of ocean-atmosphere feedbacks in the climate system. Three models were selected: CNRM-ESM2-1, HadGEM3-GC31-LL and UKESM1-0-LL.

Finally, to explain an increase in the dust emission in the Middle East, three types of data were examined. (1) We used the global Met Office Integrated Data Archive System Land and Marine Surface Station data from 1990 to 2009 (UK Meteorological Office, 2016) (UKMIDAS), available from the British Atmospheric Data Centre. Following Shao et al. (2013), we counted days of blowing dust and dust storm for each station. For a given station, a blowing dust day is defined as a day with a record of ww (weather code) =7 (raised dust or sand with visibility of 1-10 km); a dust storm day is

the day with a record of ww=9 or 30–32 (strong winds lift large quantities of dust particles, reducing visibility to between 200 and 1000 m). We averaged blowing dust days and dust storm days of all stations as the days of each dust weather in the Middle East. Because of few records of dust storm at stations, only blowing dust day was analyzed in this study. (2) The Global Precipitation Climatology Project (GPCP) data from 1979 to the present has been utilized to examine the changes in soil moisture in the Middle East. The GPCP provides monthly global precipitation from the integration of various satellite datasets of lands and oceans and a gauge analysis over land, with 2.5°×2.5° horizontal resolution (Adler et al., 2017). (3) To examine the changes in the frequency of cyclone in the Middle East, cyclone was recognized by the JRA-55 Reanalysis dataset and its frequency was counted. According to the objective cyclone tracking algorithm (Blender et al, 1997; Wang et al, 2013), the geopotential height field at 1000 hPa was used as the analysis field. The center of cyclones was found by determining the local minimum of geopotential height. Then the region around the center point of cyclones with a radius of 1000 km was evenly divided into eight areas based on the grid point. When at least one grid point in each area is 50 gpm greater than the center point, a cyclone was recognized. We counted the frequency of cyclones every 6 hours in the Middle East.

In this study, dust in spring (March to May) was analyzed, because there was more dust in spring than in other seasons over the TP (Liu et al., 2008). In addition, due to the limited period of the MERRA-2 Reanalysis dataset, only data in 1980-2017 was analyzed. Equally, other data such as the simulations of the CESM and the CIMP6, the ice core data, cyclone frequency, and the GPCP were examined in spring during 1990-2010.

3. Increased dust aerosols over the TP during 2000s

Figure 1 presents the climatology of dust optical thickness (DOT) during the

spring from 1990 to 2009 over the TP and its marginal regions. The TP in China ranges from 26°00′12″ N to 39°46′50″ N and from 73°18′52″ E to 104°46′59″ E (Zhang et al., 2002). There is high DOT over the Taklimakan Desert, Tsaidam Basin, and the northern area of South Asia, with values above 0.18. The DOT over the TP is lower than that over those regions with values ranging from 0.02-0.08. Moreover, there are obvious spatial differences in the DOT over the TP. There are more dust aerosols over the northern portion of the TP than the southern portion. The DOT over the north is 0.04-0.1, and that over the south is 0.02-0.04, which is supported by the dust aerosol observations from the remote sensing datasets (Gong et al., 2012; Huang et al., 2007). We used the mean of atmospheric dust aerosols in the red rectangle shown in Figure 1 to represent the atmospheric dust aerosols over the TP (80°E-100°E, 30°N-36°N).

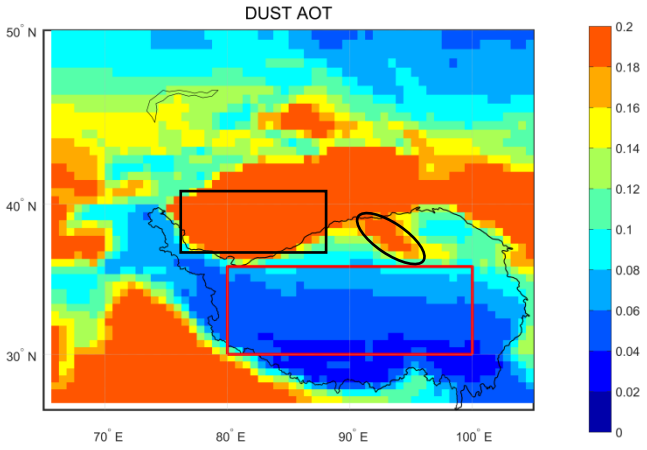

Figure 1. The climatology of spring dust aerosol optical thickness (DOT) during 1990 to 2009 over the Tibetan Plateau (TP) and its marginal regions (March to May). Study area is shown in a red rectangle (80°E - 100°E, 30°N - 36°N), which is used to represent the TP in this paper. The region in the black rectangle (oval) indicates the Taklimakan Desert (Tsaidam Basin).

Figure 2 shows the variation of monthly averaged DOT over the TP from 1980-2017. The DOT over the TP increases from January to April and May, and then it decreases gradually for the rest of the year. The monthly averaged DOT in the 2000s (2000-2009, P2) are slightly higher than those in the 1990s (1990-1999, P1). The

seasonal averages of DOT in springs and summers during 1990-2009 are shown in Figure 2k and Figure 2l, respectively. It is evident that there are significant differences in DOT between the P1 and P2 time periods during springs and summers. The averaged DOT is 0.05 (0.04) and 0.07 (0.05) during P1 and P2, respectively, for the spring (summer) seasons. The differences in DOT between P1 and P2 (P2 minus P1) are 0.017 and 0.011 in spring and in summer, respectively, which are significant at the 95% confidence level. The DOT over the TP during the spring is higher in P2 than P1 by 36%. In addition, the increased dust aerosols over the TP during the P2 period are consistent with the ice core records. The annual deposition flux as measured in Tanggula, Guliya, and Mugagangqiong ice cores increased from 1990 to 2011 (Gong et al., 2012; Thompson et al., 2018). Next, we will investigate the possible causes for the increases in dust aerosols over the TP during the 2000s.

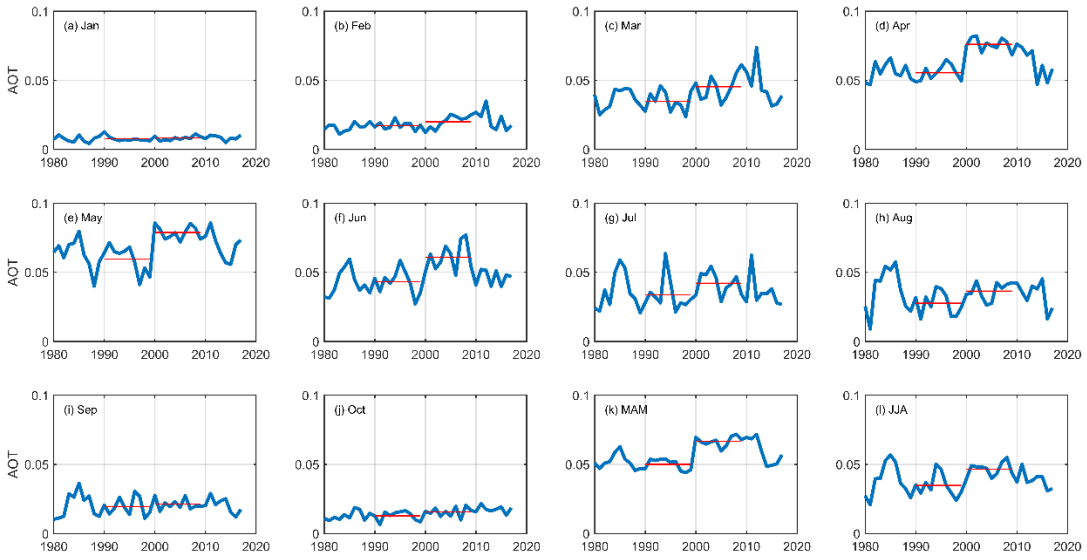

Figure 2. Variation of monthly dust aerosol optical thickness (DOT) during 1980 – 2017 over the TP. (a) - (j) are for January to October. (k) and (j) represent spring and summer DOT, respectively, averaged over March to May and June to August. Red lines represent the DOT average of 1990-1999 (P1) and 2000-2009 (P2), respectively.

4. The significant contribution of remote dust sources to increased dust over the TP during the 2000s

The dust event records at surface stations on the TP show lower frequency of dust event during P2 than during P1 (Kang et al., 2016), which is opposite to the variation in the DOT derived from the MERRA-2 Reanalysis dataset. This means that the increased atmospheric dust over the TP during P2 may be related to increased dust transportation from potential remote dust sources. We first calculated the distribution of spring dust emissions in the MERRA-2 Reanalysis dataset (P2 minus P1, figures 3a). As seen in the figure 3a, there are increased dust emissions of 0.1×10^{-5} $g\cdot m^{-2}\cdot s^{-1}$ over the eastern North Africa, 0.15×10^{-5} $g\cdot m^{-2}\cdot s^{-1}$ over the northern Arabian Peninsula in the Middle East, and 0.05×10^{-5} $g\cdot m^{-2}\cdot s^{-1}$ over the northwestern TP during the P2 than the P1. It means that eastern North Africa, the Middle East, and the northwestern TP may be potential sources for the increase in the atmospheric dust over the TP during 2000s. However, because of anomalous downward flows from middle troposphere to the surface over eastern North Africa and northwestern TP (figure 1, figure 2 and figure 3 in supplementary material), these regions are not possible to contribute more dust to the TP. Only the northern Arabian Peninsula in the Middle East is likely the potential source for the increasing dust aerosols over the TP. We averaged the dust emissions in the northern Arabian Peninsula in the Middle East (35°E - 65°E, 25°N - 35°N) for the period of 1990-2009 (figure 3c). The dust emissions increased by 4.3% during the P2 than P1.

Figure 3b shows the spatial distribution of spring blowing dust days between 1990s and 2000s over the Middle East and the Central Asia derived from the UKMIDAS data. The blowing dust days in spring increased largely in northern Arabian Peninsula and northern Iranian Plateau during the P2 compared to the P1. In the meantime, some stations in the rest part of the Middle East are featured by weak decease in the blowing dust days in spring during the P2 than the P1. We averaged the blowing dust days in spring over the northern Arabian Peninsula and northern Iranian plateau during 1990-2009; the blowing dust days increased by 58.4% during the P2 than the P1

(figure 3d). In sum, the increased blowing dust days in the Middle East during the P2 may result in the increase of dust emissions over these regions in this period. Then the increased dust may lead to the increase in the atmospheric dust over the TP during the P2 through a long-distance transport.

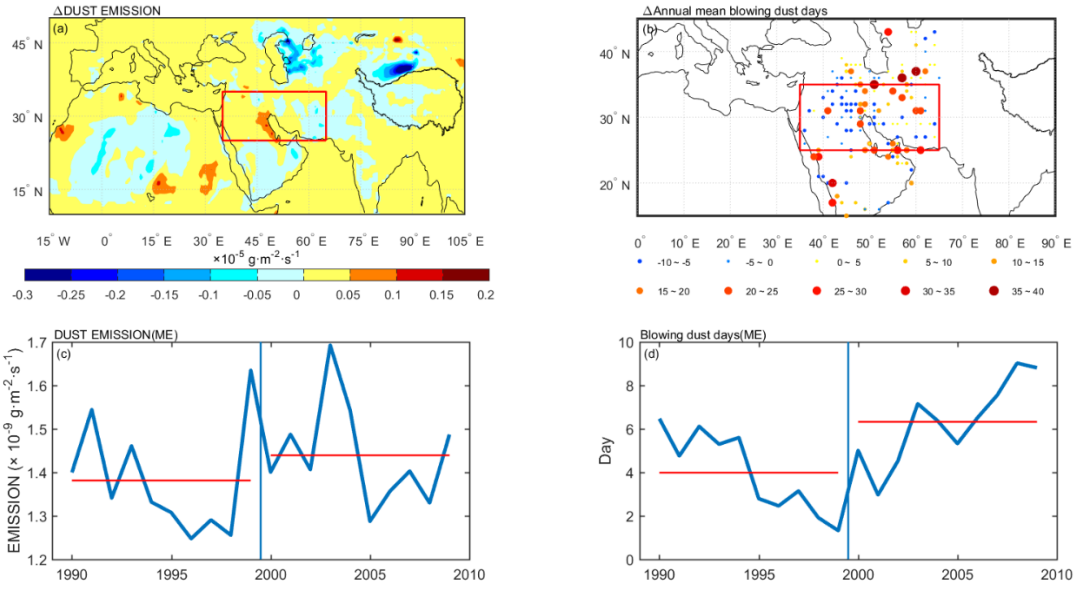

Figure 3. Distribution of spring dust emission (a), annual mean blowing dust days (b) between 2000-2009 and 1990-1999 (the former minus the latter). The red rectangle is for the Middle East. And variations of spring dust emission (c), and blowing dust days (d) over the Middle East. The dust emission (unit: $g \cdot m^{-2} \cdot s^{-1}$) is based on MERRA-2 data and blowing dust days are indicated by UKMIDAS data during 1990–2009.

5. Causes of increased dust transportation from the Middle East to the TP during the 2000s

In this section, we first examined changes in precipitation to recognize the role of surface conditions in increases in dust transportation from the Middle East to the TP. Second, variation in cyclones was discussed in order to explain how dust is uplifted from the surface to the middle troposphere over the Middle East. Finally, we analyzed

232 the variations in atmospheric circulation in the middle troposphere that are responsible
233 for dust transport from sources to the TP.
234
235 **5.1 Drying surface and increased cyclone activities over the Middle East**
236
237 Surface conditions play an important role in the formation of dust weather and
238 dust emissions. If there is less precipitation in a place, surface dust emissions will be
239 easily generated from dry and dusty ground by the action of atmospheric circulation.
240 The more that dust is emitted from the surface, the more dust is transported to the
241 middle and upper troposphere and thereafter downstream by zonal winds. The
242 difference in precipitation between P1 and P2 is shown in Figure 4. Seasonal
243 precipitation in the Middle East is lower during P2 than P1 by 0-20 mm. Based on the
244 above results, decreases in precipitation should play a role in increasing dust emissions
245 over the Middle East during the 2000s. Meanwhile, precipitation over the TP is higher
246 during P2 than P1 by 0-20 mm. This increased precipitation indicates increased surface
247 humidity and decreased dust emissions on the TP, further verifying that increased dust
248 aerosols over the TP during the 2000s are associated with remote dust sources.
249

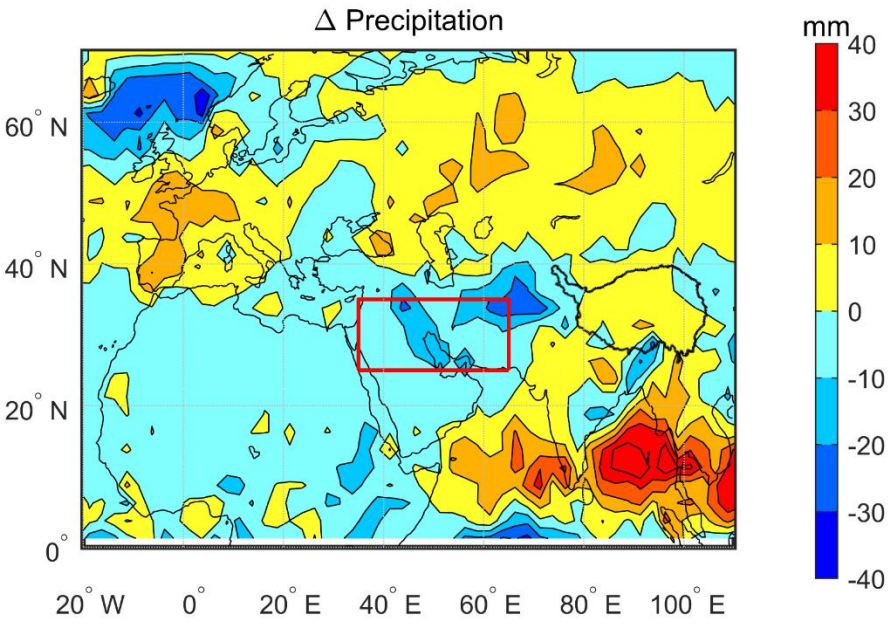

250

Figure 4. Composite of spring precipitation between 2000-2009 and 1990-1999 (the former minus the latter). The red rectangle is for the Middle East.

Many studies indicated that cyclones play important roles in the formation of dust weather over Middle Asia (Hamidi et al., 2014). We averaged the number of cyclones in spring over the Middle East during the period of 1990-2009. Figure 4 demonstrates that the number of cyclones increases more than 25.8% in the P2 compared with the P1 during springs over the Middle East. The strong winds brought by cyclones provide favorable dynamic conditions for the occurrence of blowing dust. In addition, because air flows converge at low altitude and diverge at high altitude, the air around the cyclone centers rises and the upward movement of air is conducive to the upward transportation of dust. Therefore, the increase in the cyclone number supports rising dust emissions over the Middle East during P2.

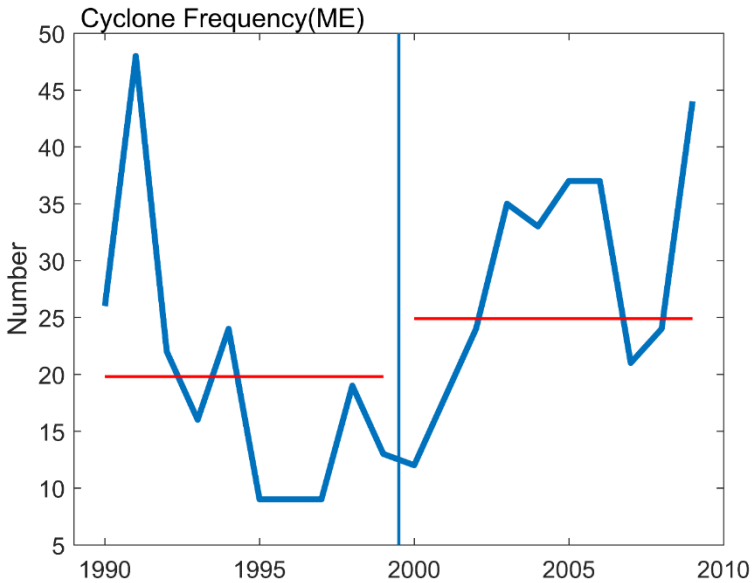

Figure 5. Variations of spring cyclone frequency during 1990 to 2009 over the Middle East. The red lines represent the average of cyclone frequency during 1990-1999 and 2000-2009, respectively.

5.2 Enhanced dust updrafts from the surface to the middle troposphere over the Middle East

We investigated the meridional mean cross-section of anomalies in the dust mixing ratio, zonal wind, meridional wind, and vertical motion over the Middle East (figure 6). Enhanced updrafts are observed from 25°N to 30°N over the Middle East. This intensified rising circulation may lift surface dust from these semiarid/arid areas to the middle and high troposphere, supported by anomalies in the dust mixing ratio with high values, ranging from 20°N to 50°N and from the surface to 5000 meters above sea level and with an anomalous center over the Middle East (25°N to 35°N). In the middle troposphere there are southward wind anomalies stretching from 30°N to 50°N that increase the transport of dust aerosols from the Arabian Peninsula to the mid-latitude regions. According to high values for the dust mixing ratio and enhanced updrafts over the Middle East, it can be concluded that the Middle East is the remote dust source for the increasing dust aerosols over the TP during the P2 years.

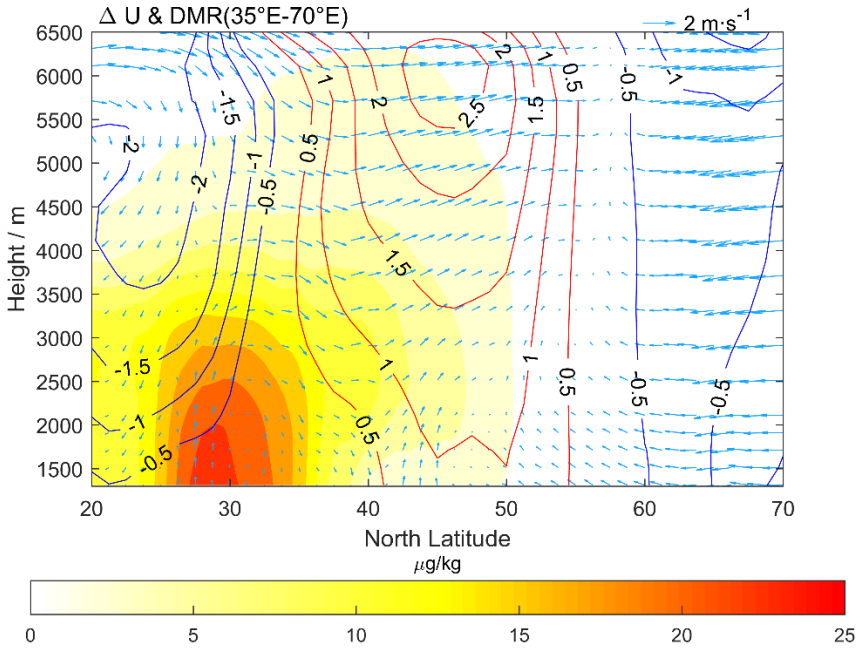

Figure 6. The mean cross-section of dust mixing ratio anomaly (shaded areas), zonal wind anomaly (contour lines), and meridional and vertical wind anomaly (arrows) between 2000-2009 and 1990-1999 (the former minus the latter) averaged over 35°E-70°E. For clarity, the vertical velocity is magnified by 100. Units: $m \cdot s^{-1}$ is for zonal and

meridional wind, $pa \cdot s^{-1}$ is for vertical wind and μg/kg is for dust mixing ratio.

In the meantime, the zonal wind anomaly presents an enhanced westerly jet during the P2 compared with the P1 during spring, indicated by an increase in zonal winds between 35°N and 60°N. On one hand, the enhanced westerly jet causes increased downward momentum transfer denoted by the contour line of a 1 $m \cdot s^{-1}$ zonal wind anomaly between 35°N-55°N below the 700 hPa level, which benefits the development of dust weather by increasing the magnitude of winds near the surface. On the other hand, once dust aerosols are uplifted into the middle and high troposphere over the mid latitudes, the enhanced westerly winds during the P2 will transport dust eastward more efficiently.

5.3 Increased dust transportation in the middle troposphere from remote dust sources to the TP

Zonal winds in the middle troposphere play important roles in transporting dust eastward from Central Asia to the TP (Mao et al., 2019). We first analyzed the composite of zonal winds averaged at 500 hPa between P1 and P2 (P2 minus P1, figure 4 in supplementary material). The positive anomalies are observed from Eastern Europe across Central Asia to Northwest China. Meanwhile, there are negative anomalies horizontally located from North Africa to South Asia. The positive anomalies in zonal winds imply an enhanced zonal wind in the middle latitudes over Central Asia, which is consistent with the strengthened westerly jet in figure 6. The enhanced westerly winds in the middle latitudes will transport dust eastward more efficiently to Northwest China.

We analyzed the composite of meridional winds over Eurasia between the P1 and P2 (P2 minus P1) to highlight the meridional transport of dust from Northwest China to the TP (figure 7). As shown in the figure, there are positive anomalies stretching from the Arabian Peninsula to the Caspian Sea and negative anomalies covering South Asia,

the TP, and the Taklimakan Desert, which are significant at the 95% confidence level. The positive anomalies of meridional wind reveal increased southerly winds from the Middle East to Central Asia, which is consistent with southerly wind anomalies from 30°N to 50°N as depicted in figure 6. Therefore, there may be more dust transported from the Middle East to Central Asia during P2 as compared with P1. Negative anomalies in the meridional wind over Pakistan, northwest India, the western TP, and the Taklimakan Desert imply that there are enhanced northerly winds across these areas during P2 compared with P1, which help induce the movement of more dust aerosols toward the TP.

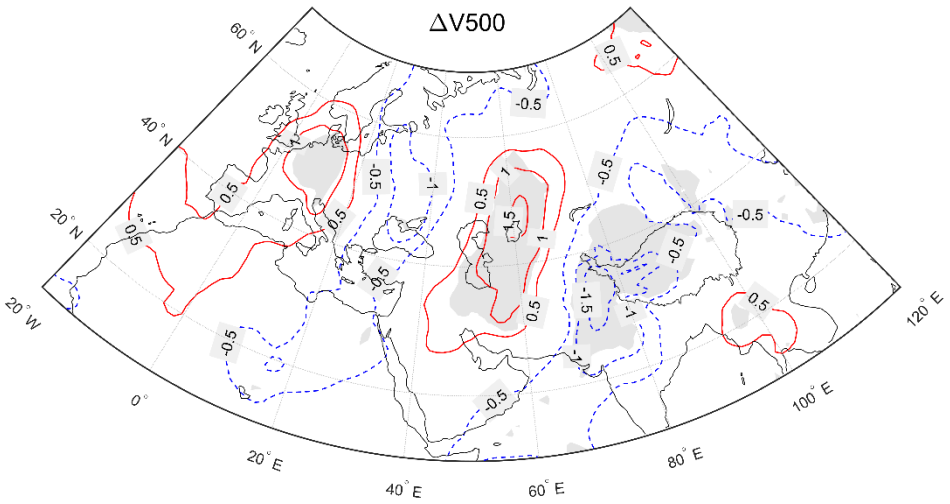

Figure 7. Composite of spring 500 hPa meridional wind between 2000-2009 and 1990-1999 (the former minus the latter). Positive (negative) values are indicated by red solid (blue dashed) lines and the shaded areas are for anomalies significant at the 95% confidence level.

6. Discussion

Aerosol optical depth (AOD) assimilated by the MERRA-2 Reanalysis dataset are different before and after 2000 (Gelaro et al., 2017). The MERRA-2 Reanalysis merges reflectance from the Advanced Very High Resolution Radiometer AVHRR (1979–2002, ocean-only) before 2000 and that from the Moderate Resolution Imaging

Spectroradiometer on Terra (2000–present) and Aqua (2002–present) after 2000. In the meantime, the MERRA-2 Reanalysis dataset merges the AOD retrievals from the Multiangle Imaging Spectro-Radiometer (2000–2014, bright, desert regions only) and direct AOD measurements from the ground-based Aerosol Robotic Network. We wonder whether the increase in the atmospheric dust over the TP during 2000s compared to 1990s is caused by different AOT data assimilated by the MERRA2 reanalysis before and after 2000. Therefore, we used dust data from ice core records, dust simulations from the CESM model, the AI from EP TOMS and three models (CNRM-ESM2-1, HadGEM3-GC31-LL, and UKESM1-0-LL) from the AMIP of the CMIP6 to verify the increase of dust aerosols over the TP from 1990 to 2010 revealed by the MERRA-2 data.

Figure 8a shows an increase in the spring dust deposition flux from P1 to P2 in the MGGQ and Tanggula ice cores. The dust deposition flux increases by 157% (46%) in MGGQ (Tanggula) ice core from the P1 to the P2, featured by an average of 47 and 121 (193 and 281) $\mu g \cdot cm^{-2}$ during P1 and P2 in the MGGQ (Tanggula) ice core, respectively. The difference in the average of spring dust deposition flux between P1 and P2 is significant at the 95% confidence level for the MGGQ and Tanggula ice core. Next, the dust AOD over the TP from the CESM model shows an upward trend from P1 to P2 (figure 8b); the trend is 0.0787 per spring, significant at the 95% confidence level. In addition, the AI in the study area over the TP increases by 69% from the 1997-1999 to the 2000-2004, featured by an average of 0.45 and 0.54 during P1 and P2, which is significant at the 95% confidence level (figure 8c). Finally, we analyzed the trends in the ensemble mean of dust concentration in the high troposphere (averaged between 400hPa and 300 hPa) over the TP from CNRM-ESM2-1, HadGEM3-GC31-LL, and UKESM1-0-LL models. Although the CNRM-ESM2-1 model shows weak increasing trend in the ensemble mean of dust concentration in the upper troposphere over the TP (figure 6 in supplementary material), the ensemble mean of dust concentration of two models (HadGEM3-GC31-LL and UKESM1-0-LL) has an upward trend from 1990 to

2009 by 0.0105×10^{-9} kg·m^{-3}·yr^{-1}and 0.0166×10^{-9} kg·m^{-3}·yr^{-1} per spring (figure 9). Thus, the increase in the dust deposition flux in the ice core, the dust AOD from the CESM model, the AI from TOMS and the dust concentration from CMIP6 models supports that the dust in the high troposphere over the TP increases in spring from 1990s to 2000s.

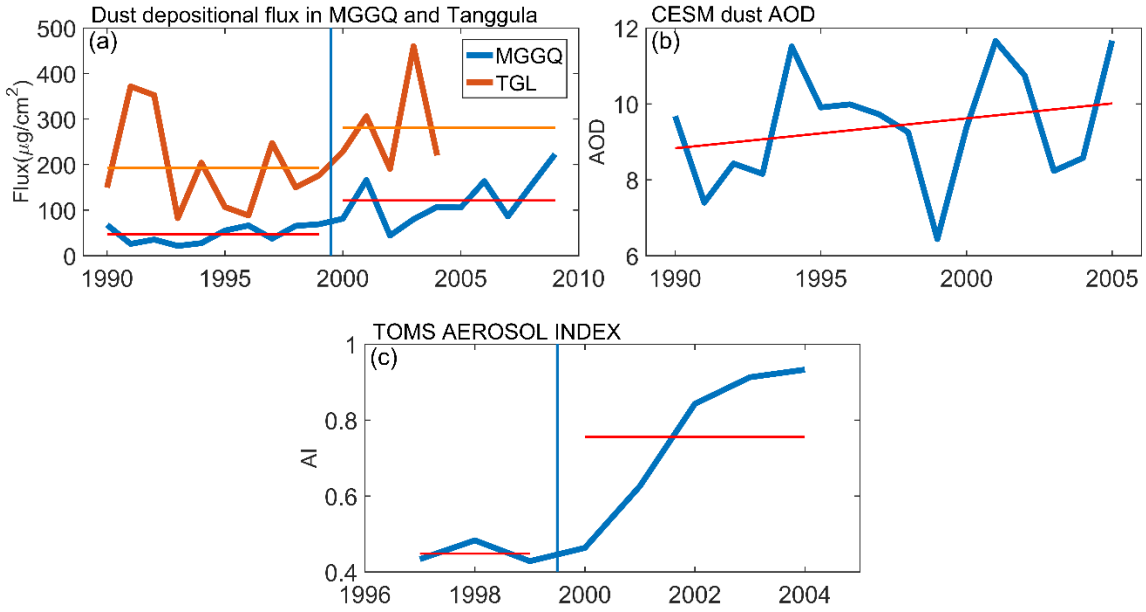

Figure 8. Variations of spring dust deposition flux from ice cores drilled at Mugagangqiong (MGGQ, 1990-2009) and Tanggula (1990-2004) (a). (b) shows the time series of dust AOD during 1990–2005 over the Tibetan Plateau from the CESM simulations; linear trend of dust AOD is indicated by a red line in (b). And (c) shows the variations of spring AI during 1997-2004. In (a), red (yellow) lines represent the average of dust deposition flux in MGGQ (Tanggula) during 1990-1999 and 2000-2009 (2000-2004). In (c), red lines represent the average of AI during 1997-1999 and 2000-2004.

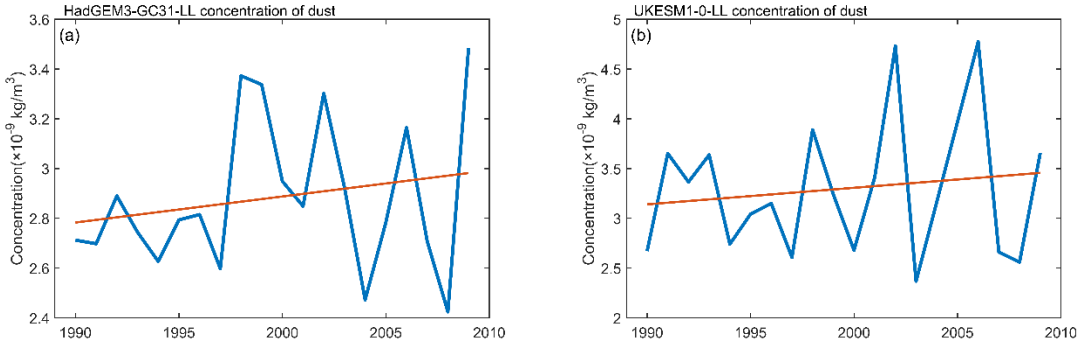

Figure 9. Time series of the ensemble mean of spring dust concentration averaged between 400 hPa and 300hpa over the TP in 1990-2009. (a) is obtained from the HadGEM3-GC31-LL model, and (b) is from UKESM1-0-LL model. Linear trends of dust concentration are shown by red lines.

7. Conclusion

This study reveals that dust in the high troposphere over the TP during springs increases in the 2000s, based on the Modern-Era Retrospective Analysis for Research and Applications, Version 2 (MERRA-2) aerosol dataset. The dust optical thicknesses (DOT) over the TP in the 2000s are higher than those in 1990s by greater than 34%. The result is supported by an increase of 157% (46%) in the spring dust deposition flux in the Mugagangqiong (Tanggula) ice core and an increase of 69% in the spring AI from EP TOMS, as well as by an increasing trend in dust aerosol optical depth over the TP from the CESM model and the ensemble mean of dust concentration in the high troposphere over the TP from the CMIP6 models. Although there are several potential sources for the dust aerosols over the TP, the increasing DOT over the TP during 2000s may be related to increasing dust emissions over the Middle East, considering the decreasing amounts of dust aerosols over the Taklimakan. Increases in dust emissions over the Middle East are caused by a decrease in precipitation and an increase in cyclonic activity from the 1990s to the 2000s. The frequency of cyclones over the Middle East increases over 25.8% from the 1990s to the 2000. More cyclone activity

may uplift more dust aerosols from the surface to the middle troposphere by intensified rising circulation. Finally, during the 2000s, the atmospheric circulation in the middle troposphere over the Eurasia is beneficial to more dust aerosols over the TP. The enhanced mid-latitude westerlies transport more dust aerosols eastward to Northwest China and thereafter increases in northerly winds over Northwest China propel dust southward to the TP.

Acknowledgments. The research was supported by the National Key R&D Program of China (2016YFA0602401). Mao was supported by the National Natural Science Foundation of China (41571039). Zhao was supported by the National Natural Science Foundation of China (91837204). MERRA-2 data are obtained from NASA Goddard Earth Sciences (GES) Data and Information Services Center (DISC; https://gmao.gsfc.nasa.gov/reanalysis/merra-2/). JRA-55 data are obtained from the Japan Meteorological Agency (JMA; https://jra.kishou.go.jp/JRA-55/). GPCP Precipitation data are provided by the NOAA/OAR/ESRL PSD, Boulder, Colorado, USA (https://www.esrl.noaa.gov/psd/). TOMS data are produced by the Laboratory for Atmospheres at NASA Goddard Space Flight Center (https://disc.gsfc.nasa.gov/datasets/TOMSEPL3maer_008/). UKMIDAS data are available from the British Atmospheric Data Centre (http://data.ceda.ac.uk/badc/ukmo-midas/). Simulated AMIP data from the World Climate Research Programme (WCRP) CMIP6 are accessed from the website at https://esgf-node.llnl.gov/search/cmip6/. CESM data are stored in the super-blade computing system at the Institute of Atmospheric Physics, Chinese Academy of Sciences, and they are available upon request from Chenglai Wu (wuchenglai@mail.iap.ac.cn). And the ice core records are available upon request from Guangjian Wu (wugj@itpcas.ac.cn).

References

Adler, R. F., Sapiano, M., Huffman, G. J., Wang, J. J., Gu, G., Bolvin, D., el al. (2018), The Global Precipitation Climatology Project (GPCP) Monthly Analysis (New Version 2.3) and a Review of 2017 Global Precipitation, *Atmosphere (Basel)*, 9(4), 138. https://doi.org/10.3390/atmos9040138

Blender, R., K. Fraedrich, & F. Lunkeit (1997), Identification of cyclone track regimes in the north Atlantic, *Quarterly Journal of the Royal Meteorological Society*, 123(539), 727-741. https://doi.org/10.1002/qj.49712353910

Chen, S., J. Huang, C. Zhao, Y. Qian, L. R. Leung, & B. Yang (2013), Modeling the transport and radiative forcing of Taklimakan dust over the Tibetan Plateau: A case study in the summer of 2006[J], *Journal of Geophysical Research: Atmospheres*, 118(2), 797-812. https://doi.org/10.1002/jgrd.50122

Diop, D., Kama, A., Drame, M. S., Diallo, M., & Niang, D. N. (2018), The use of aladin model and merra-2 reanalysis to represent dust seasonal dry deposition from 2006 to 2010 in senegal, west africa, *Modeling Earth Systems and Environment*, 4, 815-823. https://doi.org/10.1007/s40808-018-0458-5

Forster, P., Ramaswamy, V., Artaxo, P., Berntsen, T., Betts, R., Fahey, D.W., el al. (2007), Changes in Atmospheric Constituents and in Radiative Forcing. In: Climate Change 2007: The Physical Science Basis. Contribution of Working Group I to the Fourth Assessment Report of the Intergovernmental Panel on Climate Change [Solomon, S., Qin, D., Manning, M., Chen, Z., Marquis, M., Averyt, K.B., Tignor, M. & H.L. Miller (eds.)]. Cambridge University Press, Cambridge, United Kingdom and New York, NY, USA.

458

459 Eyring, V., S. Bony, G. A. Meehl, C. A. Senior, B. Stevens, R. J. Stouffer, & K. E. Taylor
460 (2016), Overview of the Coupled Model Intercomparison Project Phase 6 (CMIP6)
461 experimental design and organization, *Geoscientific Model Development*, 9(5),
462 1937-1958. https://doi.org/10.5194/gmd-9-1937-2016

463

464 Gao, H. & Washington R. (2010), Arctic oscillation and the interannual variability of
465 dust emissions from the Tarim Basin: a TOMS AI based study, *Climate Dynamics*,
466 35(2-3), 511-522. https://doi.org/10.1007/s00382-009-0687-4

467

468 Gelaro, R., McCarty, W., Suarez, M. J., Todling, R., Molod, A., Takacs, L., & Wargan,
469 K. (2017), The Modern-Era Retrospective Analysis for Research and Applications,
470 Version 2 (MERRA-2), *Journal of Climate*, 30(14), 5419-5454.
471 https://doi.org/10.1175/JCLI-D-16-0758.1

472

473 Gong, X. Q., Wu, G. J., Zhang, C. L., Zhang, X. L., & Xu, T. L. (2012), Dust change
474 over the tibetan plateau in recent years using ice core records and satellite remote
475 sensing data, *Journal of Glaciology and Geocryology*, 34(2), 257-266.
476 http://ir.itpcas.ac.cn:8080/handle/131C11/1913

477

478 Hamidi, M., M. R. Kavianpour, & Y. Shao (2014), Numerical simulation of dust events
479 in the Middle East, *Aeolian Research*, 13, 59-70.
480 https://doi.org/10.1016/j.aeolia.2014.02.002

481

482 Han, Y., X. Fang, T. Zhao, H. Bai, S. Kang, & L. Song (2009), Suppression of
483 precipitation by dust particles originated in the Tibetan Plateau, *Atmospheric*
484 *Environment*, 43(3), 568-574. https://doi.org/10.1016/j.atmosenv.2008.10.018

485

Haywood, J., P. Francis, S. Osborne, M. Glew, N. Loeb, E. Highwood, el al. (2003), Radiative properties and direct radiative effect of Saharan dust measured by the C-130 aircraft during SHADE: 1. Solar spectrum, *Journal of Geophysical Research: Atmospheres*, 108(D18), 8579. https://doi.org/10.1029/2002JD002552

Huang, J., P. Minnis, Y. Yi, Q. Tang, X. Wang, Y. Hu, Z. Liu, K. Ayers, C. Trepte, & D. Winker (2007), Summer dust aerosols detected from CALIPSO over the Tibetan Plateau, *Geophysical Research Letters*, 34(18), 1–5. https://doi.org/10.1029/2007GL029938

Huang, J., Q. Fu, J. Su, Q. Tang, P. Minnis, Y. Hu, Y. Yi, & Q. Zhao (2009), Taklimakan dust aerosol radiative heating derived from CALIPSO observations using the Fu-Liou radiation model with CERES constraints, *Atmospheric Chemistry and Physics*, 9(12), 4011-4021. https://doi.org/10.5194/acpd-9-5967-2009

Huang, J., T. Wang, W. Wang, Z. Li, & H. Yan (2014), Climate effects of dust aerosols over East Asian arid and semiarid regions, *Journal of Geophysical Research: Atmospheres*, 119(19), 398-311. https://doi.org/10.1002/2014JD021796

Hurrell, J. W., M. M. Holland, S. Ghan, J.-F. Lamarque, D. Lawrence, W. H. Lipscomb, N. Mahowald, el al. (2013), The Community Earth System Model: A Framework for Collaborative Research, *Bulletin of the American Meteorological Society*, 94(9), 1339-1360. https://doi.org/10.1175/BAMS-D-12-00121.1

Jia, R., Liu, Y., Chen, B., Zhang, Z. J., and Huang, J. P. (2015), Source and transportation of summer dust over the Tibetan Plateau, *Atmospheric Environment,* 123, 210-219. http://dx.doi.org/10.1016/j.atmosenv.2015.10.038

514 Kang, L., J. Huang, S. Chen, & X. Wang (2016), Long-term trends of dust events over
515 Tibetan Plateau during 1961–2010, *Atmospheric Environment*, 125, 188-198.
516 http://dx.doi.org/10.1016/j.atmosenv.2015.10.085
517
518 Klose, M., Y. Shao, M. K. Karremann, & A. H. Fink (2010), Sahel dust zone and
519 synoptic background, *Geophysical Research Letters*, 37(9), 298-308.
520 http://dx.doi.org/10.1029/2010GL042816
521
522 Kobayashi, S., Ota, Y., Harada, Y., Ebita, A., Moriya, M., Onoda, H., el al. (2015), The
523 JRA-55 Reanalysis: General Specifications and Basic Characteristics, *Journal of*
524 *the Meteorological Society of Japan*. Ser. II, 93(1), 5-48.
525 https://doi.org/10.2151/jmsj.2015-001
526
527 Lau, K. M., M. K. Kim, & K. M. Kim (2006), Asian summer monsoon anomalies
528 induced by aerosol direct forcing: the role of the Tibetan Plateau, *Climate*
529 *Dynamics*, 26(7-8), 855-864. http://doi.org/10.1007/s00382-006-0114-z
530
531 Lau, W. K. M., M.-K. Kim, K.-M. Kim, & W.-S. Lee (2010), Enhanced surface
532 warming and accelerated snow melt in the Himalayas and Tibetan Plateau induced
533 by absorbing aerosols, *Environmental Research Letters*, 5(2).
534 https://doi.org/10.1088/1748-9326/ 5/2/025204
535
536 Lau, W. K., & K.-M. Kim (2018), Impact of Snow-Darkening by Deposition of Light-
537 Absorbing Aerosols on Snow Cover in the Himalaya-Tibetan-Plateau and
538 Influence on the Asian Monsoon: A Possible Mechanism for the Blanford
539 Hypothesis, *Atmosphere*, 9, 438. https://doi.org/10.3390/atmos9110438
540
541 Li, P., G. Wu, X. Zhang, N. Yan, & X. Zhang (2019), Variation in atmospheric dust

since 1950 from an ice core in the Central Tibetan Plateau and its relationship to atmospheric circulation, *Atmospheric Research*, 220, 10-19. https://doi.org/10.1016/j.atmosres.2018.12.030

Liu, Y., Sato, Y., Jia, R., Xie, Y., Huang, J., & Nakajima, T. (2015), Modeling study on the transport of summer dust and anthropogenic aerosols over the Tibetan Plateau, *Atmospheric Chemistry and Physics*, 15, 12581-12594. https://doi.org/10.5194/acp-15-12581-2015

Liu, Z, Liu, D., Huang, J., Vaughan, M., Uno, I., Sugimoto, N., el al. (2008), Airborne dust distributions over the Tibetan Plateau and surrounding areas derived from the first year of CALIPSO lidar observations, *Atmospheric Chemistry and Physics*, 8(16), 5045–5060. https://doi.org/10.5194/acp-8-5045-2008

Mao, R., Gong, D. Y., Shao, Y., & Bao, J. (2013), Numerical analysis for contribution of the Tibetan Plateau to dust aerosols in the atmosphere over the East Asia, *Science China Earth Sciences*, 56(2), 301-310. https://doi.org/10.1007/s11430-012-4460-x

Mao, R., Hu, Z., Zhao, C., Gong, D. Y., Guo, D., Wu, G. j. (2019), The source contributions to the dust over the Tibetan Plateau: A modelling analysis, *Atmospheric Environment*, 214, 116859.

Qian, Y., T. J. Yasunari, S. J. Doherty, M. G. Flanner, W. K. M. Lau, J. Ming, H. Wang, M. Wang, S. G. Warren, & R. Zhang (2014), Light-absorbing particles in snow and ice: Measurement and modeling of climatic and hydrological impact, *Advances in Atmospheric Sciences*, 32(1), 64-91. https://doi.org/10.1007/s00376-014-0010-0

570 Sang, J., Kim, M.K., Lau, W. K., Kim, K. M., & Lee, W. S. (2013), Observational
571 evidence of EHP effects on the early melting of snowpack over the Tibetan Plateau
572 and Indian summer monsoon, *Egu General Assembly*, 15.
573
574 Shao, Y., Klose, M., & Wyrwoll, K. H. (2013), Recent global dust trend and connections
575 to climate forcing, *Journal of Geophysical Research: Atmospheres*, 118(19),
576 11,107-11. https://doi.org/10.1002/jgrd.50836
577
578 Sierra-Hernández, M. R., P. Gabrielli, E. Beaudon, A. Wegner, & L. G. Thompson
579 (2018), Atmospheric depositions of natural and anthropogenic trace elements on
580 the Guliya ice cap (northwestern Tibetan Plateau) during the last 340 years,
581 *Atmospheric Environment*, 176, 91-102.
582 https://doi.org/10.1016/j.atmosenv.2017.11.040
583
584 Sun, H., X. Liu, & Z. Pan (2017), Direct radiative effects of dust aerosols emitted from
585 the Tibetan Plateau on the East Asian summer monsoon – a regional climate model
586 simulation, *Atmospheric Chemistry and Physics*, 17(22), 13731-13745.
587 https://doi.org/10.5194/acp-17-13731-2017
588
589 Thompson, L. G., T. Yao, M. E. Davis, E. Mosley-Thompson, G. Wu, S. E. Porter, B.
590 Xu, el al. (2018), Ice core records of climate variability on the Third Pole with
591 emphasis on the Guliya ice cap, western Kunlun Mountains, *Quaternary Science*
592 *Reviews*, 188, 1-14. https://doi.org/10.1016/j.quascirev.2018.03.003
593
594 UK Meteorological Office (2016), Met Office Integrated Data Archive System
595 (MIDAS) Land and Marine Surface Stations Data (1853–current), [Internet].
596 NCAS British Atmospheric Data Centre, Available from
597 http://badc.nerc.ac.uk/view/badc.nerc.ac.uk_ATOM_dataent_ukmo-midas.

598
599 Wang, L. X., Y. Feng, G. P. Compo, V. R. Swail, F. W. Zwiers, R. J. Allan, & P. D.
600 Sardeshmukh (2013), Trends and low frequency variability of extra-tropical
601 cyclone activity in the ensemble of twentieth century reanalysis, *Climate*
602 *Dynamics*, 40. https://doi.org/10.1007/s00382-012-1450-9
603
604 Wu, C., Z. Lin, J. He, M. Zhang, X. Liu, R. Zhang, & H. Brown (2016), A process-
605 oriented evaluation of dust emission parameterizations in CESM: Simulation of a
606 typical severe dust storm in East Asia, *Journal of Advances in Modeling Earth*
607 *Systems*, 8(3), 1432-1452. https://doi.org/10.1002/2016ms000723
608
609 Wu, G., C. Zhang, B. Xu, R. Mao, D. Joswiak, N. Wang, & T. Yao (2013), Atmospheric
610 dust from a shallow ice core from Tanggula: implications for drought in the central
611 Tibetan Plateau over the past 155 years, *Quaternary Science Reviews*, 59, 57-66.
612 https://doi.org/10.1016/j.quascirev.2012.10.003
613
614 Yang, J., Wang, W. C., Chen, G. X., Qi, X., & Zhou, S. Y. (2018), Intraseasonal variation
615 of the black carbon aerosol concentration and its impact on atmospheric circulation
616 over the southeastern Tibetan Plateau, *Journal of Geophysical Research:*
617 *Atmospheres*. https://doi.org/10.1029/2018JD029013
618
619 Zender, C. S., H. Bian, & D. Newman (2003), Mineral Dust Entrainment and
620 Deposition (DEAD) model: Description and 1990s dust climatology, *Journal of*
621 *Geophysical Research*, 108(D14). https://doi.org/10.1029/2002jd002775
622
623 Zhang, Y. L., Li, B. Y., & Zheng, D. (2002), A discussion on the boundary and area of
624 the tibetan plateau in china. *Geographical Research*, 21(1), 1-10.
625 https://doi.org/10.1007/s11769-002-0045-5

Zhao, C. F., Yang, Y. K., Fan, H., Huang, J. P., Fu, Y. F., Zhang X. Y., el al. (2019), Aerosol Characteristics and Impacts on Weather and Climate over Tibetan Plateau, *National Science Review*, nwz184. https://doi.org/10.1093/nsr/nwz184

LIST OF FIGURES

confidence level.

Figure 8. Variations of spring dust deposition flux from ice cores drilled at Mugagangqiong (MGGQ, 1990-2009) and Tanggula (1990-2004) (a). (b) shows the time series of dust AOD during 1990–2005 over the Tibetan Plateau from the CESM simulations; linear trend of dust AOD is indicated by a red line in (b). And (c) shows the variations of spring AI during 1997-2004. In (a), red (yellow) lines represent the average of dust deposition flux in MGGQ (Tanggula) during 1990-1999 and 2000-2009 (2000-2004). In (c), red lines represent the average of AI during 1997-1999 and 2000-2004.

Figure 9. Time series of the ensemble mean of spring dust concentration averaged between 400 hPa and 300hpa over the TP in 1990-2009. (a) is obtained from the HadGEM3-GC31-LL model, and (b) is from UKESM1-0-LL model. Linear trends of dust concentration are shown by red lines.

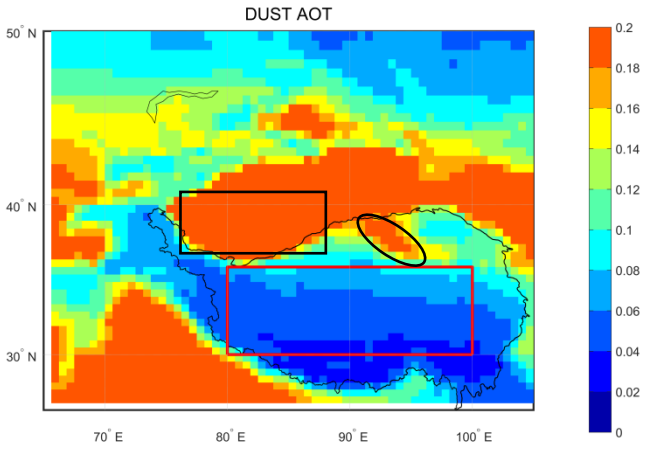

Figure 1. The climatology of spring dust aerosol optical thickness (DOT) during 1990 to 2009 over the Tibetan Plateau (TP) and its marginal regions (March to May). Study area is shown in a red rectangle (80°E - 100°E, 30°N - 36°N), which is used to represent the TP in this paper. The region in the black rectangle (oval) indicates the Taklimakan Desert (Tsaidam Basin).

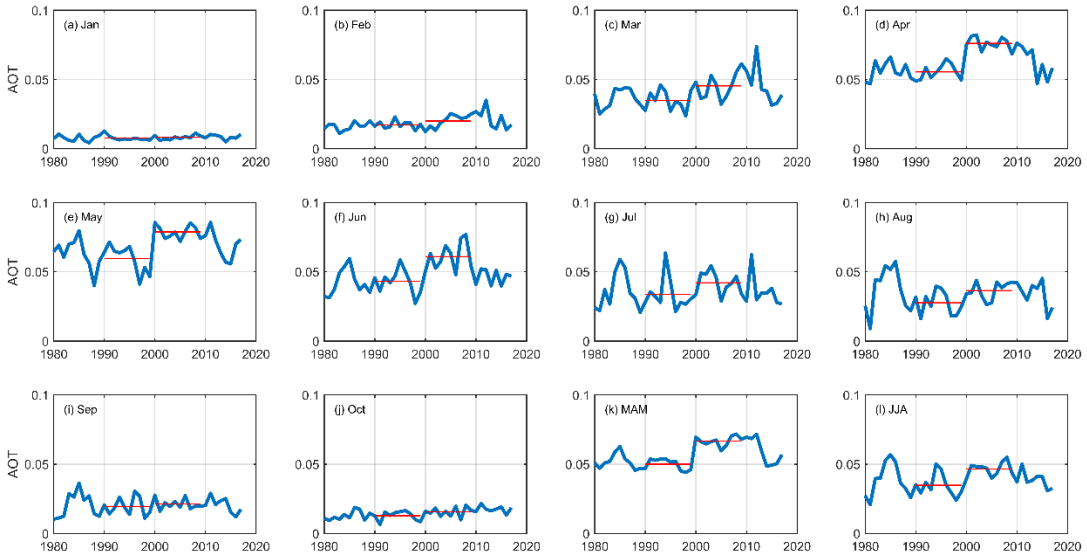

Figure 2. Variation of monthly dust aerosol optical thickness (DOT) during 1980 – 2017 over the TP. (a) - (j) are for January to October. (k) and (j) represent spring and summer DOT, respectively, averaged over March to May and June to August. Red lines represent the DOT average of 1990-1999 (P1) and 2000-2009 (P2), respectively.

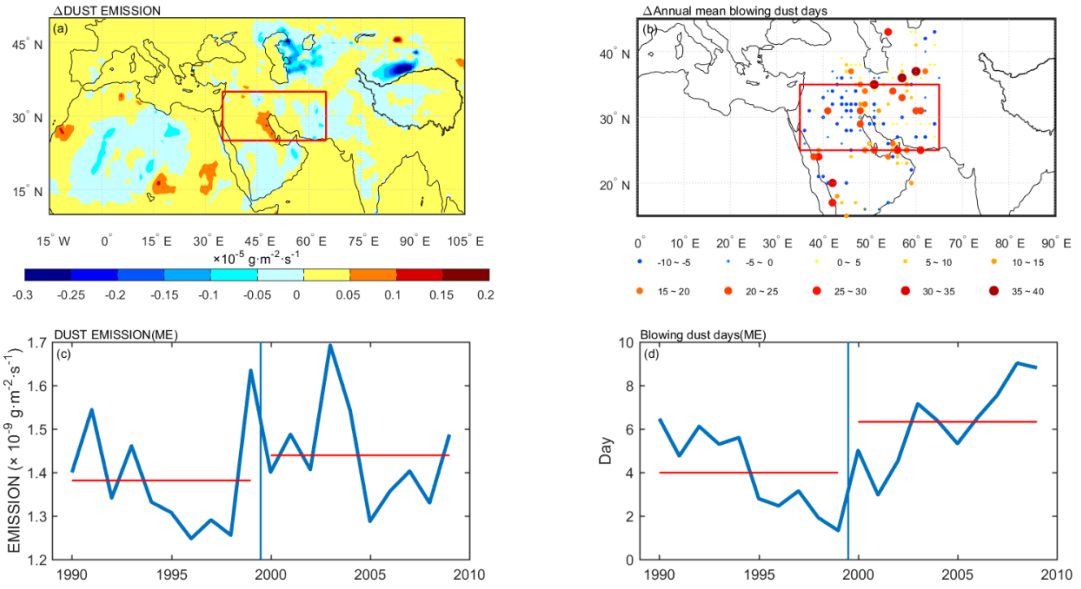

Figure 3. Distribution of spring dust emission (a), annual mean blowing dust days (b) between 2000-2009 and 1990-1999 (the former minus the latter). The red rectangle is for the Middle East. And variations of spring dust emission (c), and blowing dust days (d) over the Middle East. The dust emission (unit: $g \cdot m^{-2} \cdot s^{-1}$) is based on MERRA-2 data and blowing dust days are indicated by UKMIDAS data during 1990–2009.

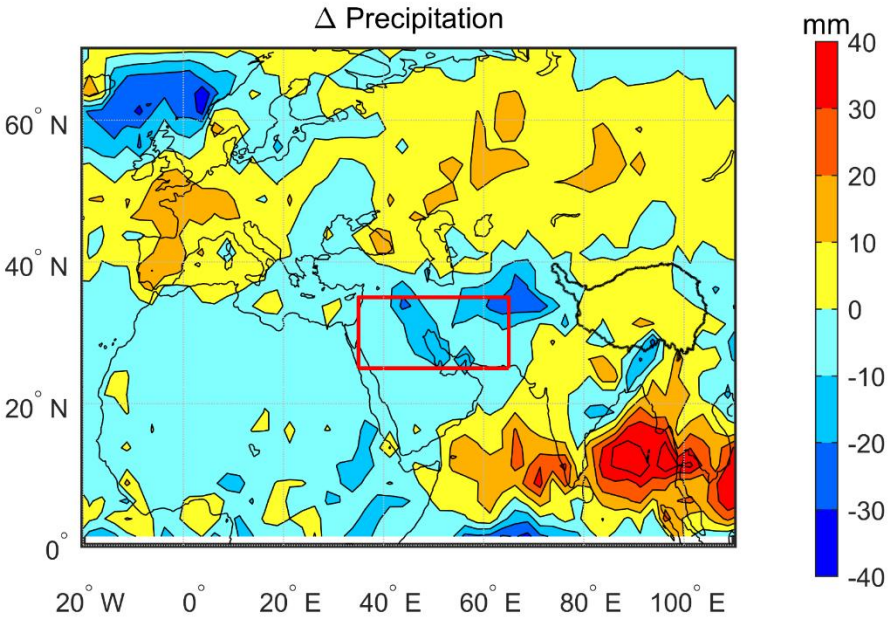

713

714 Figure 4. Composite of spring precipitation between 2000-2009 and 1990-1999 (the
715 former minus the latter). The red rectangle is for the Middle East.

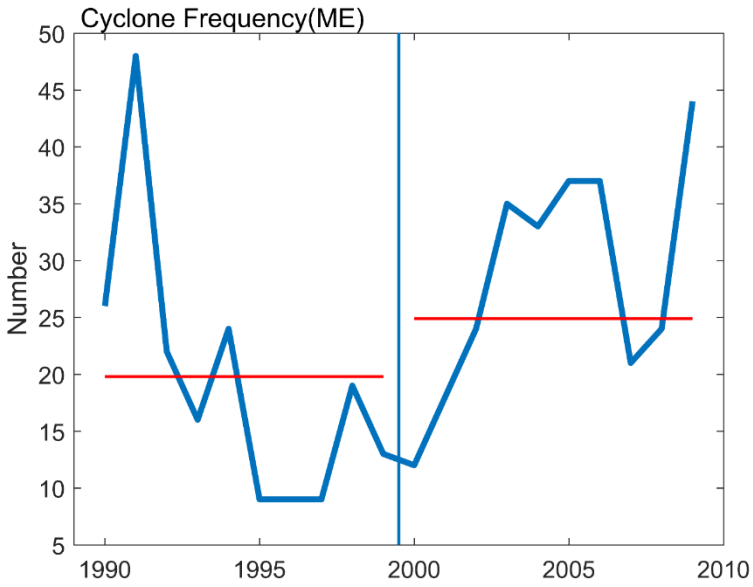

716

717 Figure 5. Variations of spring cyclone frequency during 1990 to 2009 over the Middle
718 East. The red lines represent the average of cyclone frequency during 1990-1999 and
719 2000-2009, respectively.

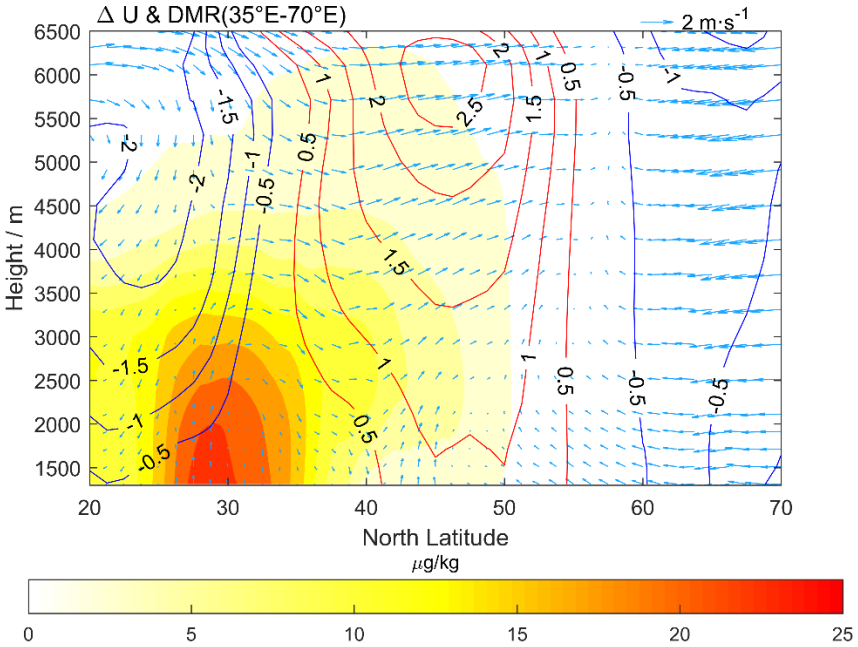

Figure 6. The mean cross-section of dust mixing ratio anomaly (shaded areas), zonal wind anomaly (contour lines), and meridional and vertical wind anomaly (arrows) between 2000-2009 and 1990-1999 (the former minus the latter) averaged over 35°E-70°E. For clarity, the vertical velocity is magnified by 100. Units: $m \cdot s^{-1}$ is for zonal and meridional wind, $pa \cdot s^{-1}$ is for vertical wind and μg/kg is for dust mixing ratio.

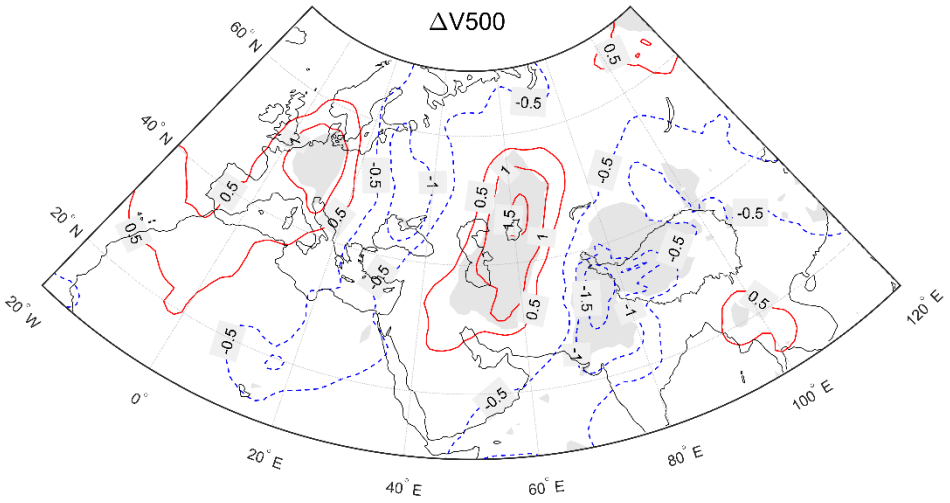

Figure 7. Composite of spring 500 hPa meridional wind between 2000-2009 and 1990-1999 (the former minus the latter). Positive (negative) values are indicated by red solid (blue dashed) lines and the shaded areas are for anomalies significant at the 95% confidence level.

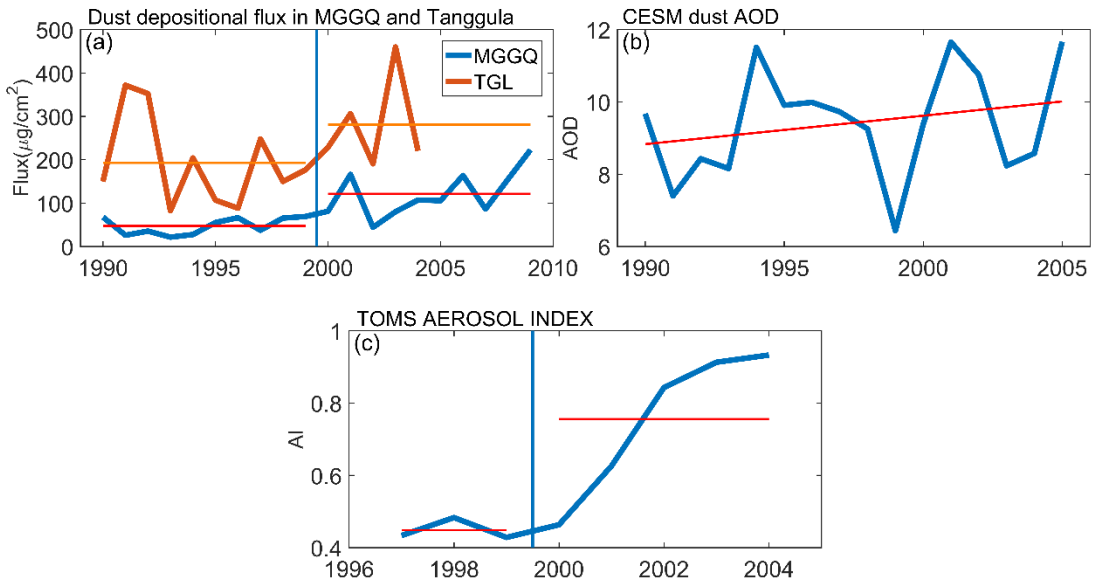

Figure 8. Variations of spring dust deposition flux from ice cores drilled at Mugagangqiong (MGGQ, 1990-2009) and Tanggula (1990-2004) (a). (b) shows the time series of dust AOD during 1990–2005 over the Tibetan Plateau from the CESM simulations; linear trend of dust AOD is indicated by a red line in (b). And (c) shows the variations of spring AI during 1997-2004. In (a), red (yellow) lines represent the average of dust deposition flux in MGGQ (Tanggula) during 1990-1999 and 2000-2009 (2000-2004). In (c), red lines represent the average of AI during 1997-1999 and 2000-2004.

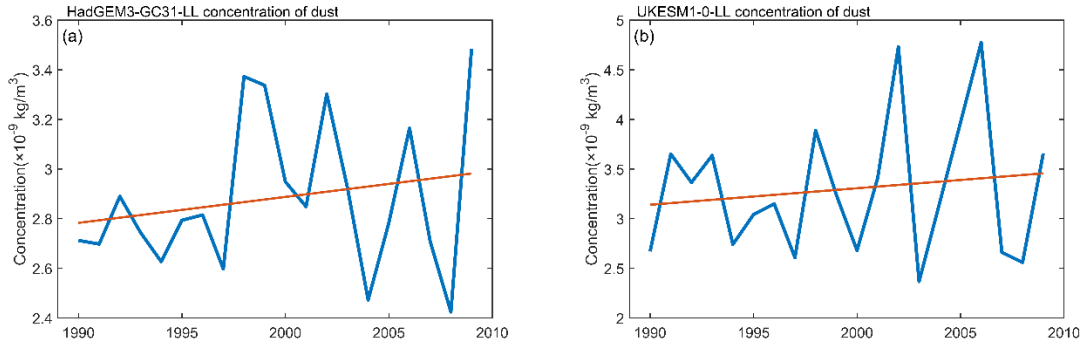

Figure 9. Time series of the ensemble mean of spring dust concentration averaged between 400 hPa and 300hpa over the TP in 1990-2009. (a) is obtained from the HadGEM3-GC31-LL model, and (b) is from UKESM1-0-LL model. Linear trends of dust concentration are shown by red lines.